The molecular face of lipid rafts in model membranes

H. Jelger Risselada and Siewert J. Marrink[1]

Groningen Biomolecular Sciences and Biotechnology Institute and Zernike Institute for Advanced Materials, University of Groningen, Nijenborgh 4, 9747 AG, Groningen, The Netherlands

Edited by Kai Simons, Max Planck Institute of Molecular Cell Biology and Genetics, Dresden, Germany, and approved September 12, 2008 (received for review August 6, 2008)

Cell membranes contain a large number of different lipid species. Such a multicomponent mixture exhibits a complex phase behavior with regions of structural and compositional heterogeneity. Especially domains formed in ternary mixtures, composed of saturated and unsaturated lipids together with cholesterol, have received a lot of attention as they may resemble raft formation in real cells. Here we apply a simulation model to assess the molecular nature of these domains at the nanoscale, information that has thus far eluded experimental determination. We are able to show the spontaneous separation of a saturated phosphatidylcholine (PC)/unsaturated PC/cholesterol mixture into a liquid-ordered and a liquid-disordered phase with structural and dynamic properties closely matching experimental data. The near-atomic resolution of the simulations reveals remarkable features of both domains and the boundary domain interface. Furthermore, we predict the existence of a small surface tension between the monolayer leaflets that drives registration of the domains. At the level of molecular detail, raft-like lipid mixtures show a surprising face with possible implications for many cell membrane processes.

coarse-grained | domain formation | liquid-ordered | molecular dynamics | polyunsaturated

According to a recent definition, rafts are small (<200 nm) heterogeneous, highly dynamic, sterol- and sphingolipid-enriched domains that compartmentalize cellular processes (1) and are believed to play an important role in cellular function (2). Although direct observation of rafts in vivo remains complicated, raft-like mixtures in model membranes can form domains that have been visualized directly for an increasing number of experimental systems and conditions (3–7). At cholesterol levels representative of biological membranes (10–30%), mixtures of saturated and unsaturated lipids separate into macroscopic domains of a liquid-ordered (L_o) phase and a liquid-disordered (L_d) phase. The first, raft-like phase is enriched in both cholesterol and the saturated lipid; the second, non-raft phase consists mainly of the unsaturated lipid and is depleted of cholesterol. In order to not confuse the reader concerning the meaning and implication of the term raft, here and throughout the remainder of this article we use the term "raft-like" phase or domain to denote the L_o phase observed in model membranes. Interestingly, isolated plasma membranes have recently been shown to be capable of forming such domains as well (8, 9). Yet it should be stressed that in real cell membranes raft formation may not resemble macroscopic phase separation. For instance, other recent experiments on plasma membranes demonstrate micrometer-scale composition fluctuations arising from critical demixing behavior (10). The focus of the current work is on phase segregation in model membranes.

To interpret the experimental measurements performed on model membranes, knowledge of the structure and dynamics of the domains at the molecular level is essential. Here we report molecular dynamics simulations of the spontaneous formation of raft-like domains in ternary lipid mixtures by using a recently developed coarse-grained (CG) lipid model, the MARTINI force field (11), which combines the speed-up benefit of simplified models (12) with the resolution obtained for atomically detailed models (13, 14). Our intermediate approach allows us to study collective processes in mixtures of realistic, i.e., physiologically important, lipids. We focus on fully hydrated mixtures of dipalmitoyl-phosphatidylcholine (diC_{16}-PC), dilinoleyl-PC ($diC_{18:2}$-PC), and cholesterol, a model system containing both a saturated and a polyunsaturated lipid component (Fig. 1*A*). Linoleic acid is a representative of the important class of ω_6 fatty acids. Experimentally, it has been shown that the presence of polyunsaturated tails increases the tendency to form domains (15, 16).

Results and Discussion

Ternary Mixtures Phase-Separate on Microsecond Time Scale. Fig. 1*B* shows the process of domain formation at the molecular level as revealed by our molecular dynamics simulations for a diC_{16}-PC/$diC_{18:2}$-PC/cholesterol 0.42:0.28:0.3 mixture containing ≈2,000 lipid molecules. Initially, the lipid components are randomized, mimicking high-temperature conditions. Subsequent quenching of the mixture to $T = 295$ K, well below the mixing temperature, leads to the rapid formation of nanoscale domains on a submicrosecond time scale. Eventually the ternary mixture completely phase separates into 2 domains spanning the simulation cell (Fig. 1*D*). Note that the formation of the striped pattern is an effect of the finite system size, which allows the domain to connect to itself across the (periodic) boundaries. Ternary mixtures of diC_{16}-PC/$diC_{18:2}$-PC/cholesterol 0.28:0.42:0.3 also completely phase-separate; however, here a circular raft-like domain is formed completely surrounded by the other domain (Fig. 1*E*). The larger area occupied by the polyunsaturated lipids prevents, in this case, the formation of the striped pattern observed for the other mixture. In accordance with the general raft hypothesis, the "green" domain contains most of the saturated lipids together with cholesterol (the raft-like L_o domain), whereas the other, "red" domain is mainly composed of the polyunsaturated lipid (the non-raft L_d domain). To mimic in vitro experiments performed on liposomes more closely, simulations have also been performed on small, unilamellar vesicles, consisting of close to 3,000 lipids in a 0.42:0.28:0.3 diC_{16}-PC/$diC_{18:2}$-PC/cholesterol ratio. Within a few microseconds, a large L_o domain assembles near one of the poles (Fig. 1*C*). Qualitatively, the properties of the L_o and L_d phases are similar for each of the 3 systems presented in Fig. 1. Because analysis of the lamellar system with the striped domain pattern is most straightforward, we focus the remaining analyses on this system.

Structure of the L_o and L_d Phases Match Experimental Data. Fig. 2*A* presents a cut through the planar diC_{16}-PC/$diC_{18:2}$-PC/cholesterol 0.42:0.28:0.3 membrane at the end of the simulation,

Author contributions: S.J.M. designed research; H.J.R. and S.J.M. performed research; H.J.R. analyzed data; and H.J.R. and S.J.M. wrote the paper.

The authors declare no conflict of interest.

This article is a PNAS Direct Submission.

Freely available online through the PNAS open access option.

[1]To whom correspondence should be addressed. E-mail: s.j.marrink@rug.nl.

This article contains supporting information online at www.pnas.org/cgi/content/full/0807527105/DCSupplemental.

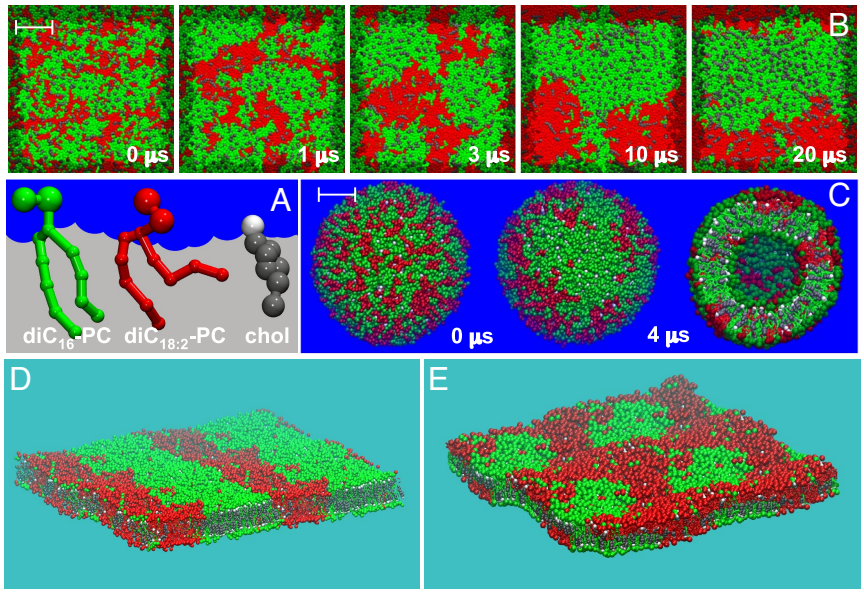

Fig. 1. Formation of L_o domains in ternary lipid mixtures. (*A*) Color coding of the lipid components. Green is used for the saturated lipids, and red is used for the polyunsaturated lipids. Cholesterol is depicted in gray with a white hydroxyl group. (*B*) Time-resolved phase segregation of a planar membrane viewed from above, starting from a randomized mixture ($t = 0$), ending with the L_o/L_d coexistence ($t = 20$ μs). (*C*) Phase segregation for the same lipid mixture in a small, 20-nm-diameter liposome. Initial ($t = 0$) and final ($t = 4$ μs, both top view and cut through the middle) configuration. (*D* and *E*) Multiple periodic images (2×2) of the phase-separated diC_{16}-PC/$diC_{18:2}$-PC/cholesterol systems show striped pattern formation in the 0.42:0.28:0.3 system (*D*) and circular domains in the 0.28:0.42:0.3 system (*E*). (Scale bar: 5 nm.)

revealing the structure (at near atomic resolution) of the 2 phases in equilibrium. The mole fraction of each of the components is quantified in Fig. 2*B*. The final composition of the raft-like L_o domain is 0.61:0.01:0.37, almost a pure binary mixture of the saturated lipid and cholesterol with only a trace amount of the polyunsaturated lipid present. The cholesterol mole fraction of 0.37 implies a moderate enrichment compared to the overall fraction of 0.3 and is still well below the solubility limit of 0.66 for cholesterol in diC_{16}-PC membranes (17). The final composition of the L_d domain is 0.08:0.75:0.17, indicating that the cholesterol mole fraction is reduced almost 2-fold with respect to a homogeneous mixture. On a qualitative level, these results agree remarkably well with the compositional analysis performed for phase-separated diC_{16}-PC/$diC_{18:1}$-PC/cholesterol vesicles, based on NMR measurements, from which it was concluded that the L_o phase is strongly enriched in the saturated

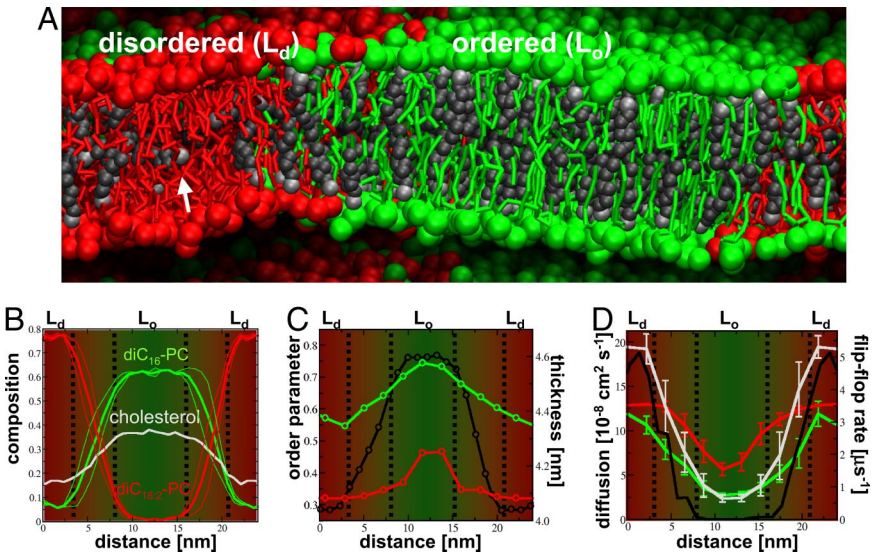

Fig. 2. Structural and dynamic properties of the 2 domains. (*A*) Side view of the planar diC_{16}-PC/$diC_{18:2}$-PC/cholesterol 0.42:0.28:0.3 system at the end of the simulation, revealing the molecular organization in both the L_o and L_d phases. The white arrow points to a cholesterol oriented in between the monolayer leaflets. (*B–D*) Various properties of the membrane along the direction perpendicular to the phase boundaries. The L_o phase is centered, flanked by 2 periodic halves of the L_d domain. A transition zone separating the 2 phases is tentatively indicated by dashed, black lines. Green, red, and gray are used to distinguish properties of diC_{16}-PC, $diC_{18:2}$-PC, and cholesterol. (*B*) Composition of the membrane expressed as a mole fraction of each of the 3 components. Thin lines represent the 2 monolayers separately; the thicker line represents the average. (*C*) Average tail order parameter for PC lipids (left axis) and membrane thickness (black curve, right axis). (*D*) Lipid lateral diffusion rate (left axis) and cholesterol flip-flop rate (black curve, right axis).

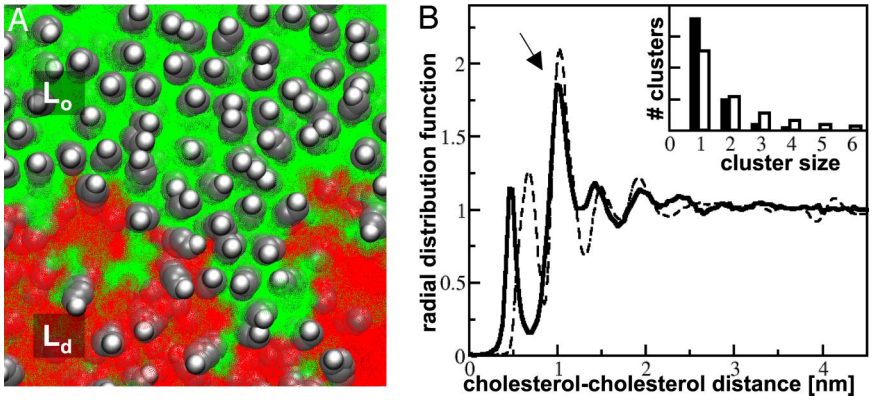

Fig. 3. Lateral organization of cholesterol in the L_o phase. (*A*) Top view of the planar membrane illustrating the typical instantaneous cholesterol organization across the raft-like phase and the boundary zone. The green and red backgrounds represent the positions of the saturated and unsaturated lipids. (*B*) Cholesterol–cholesterol radial distribution function with a solvent-separated peak at a distance of 1 nm (arrow). Results obtained from the current study are displayed by the solid line; results based on all-atom simulations (13) are shown by the dashed line for comparison. (*Inset*) Frequency distribution of cholesterol cluster sizes obtained from the simulation (solid bars) compared to a random distribution (open bars).

lipid and moderately enriched in cholesterol (18). A more quantitative comparison is difficult, because the precise composition of the domains is highly state-dependent, especially on the vicinity of the critical point.

As a consequence of the compositional differences between the 2 domains, both structural and dynamic properties of the domains differ significantly. Fig. 2*C* shows the average lipid tail order parameter and the membrane thickness as a function of the position with respect to the domain boundary. The order parameter indicates disorder of the L_d domain, whereas the L_o domain is characterized by a strong order approaching that of a gel phase. The unsaturated lipids, which are occasionally present in the raft domain, are also seen to adapt more ordered conformations. As a result of the increased order in the raft-like domain, a concomitant increase in bilayer thickness is observed, from 4.0 nm in the disordered phase to 4.6 nm in the ordered phase. The increase in bilayer thickness of 0.6 nm between the L_o and L_d phase is in quantitative agreement with atomic force microscopy (19) and NMR (16) data as well as with results from atomistic simulations (13). The area/lipid (data not shown) follows the opposite trend, increasing from 0.4 nm^2 in the L_o phase to 0.58 nm^2 in the L_d phase.

Dynamic Properties Show Relative Fast Mobility of Cholesterol. The lateral diffusion rates in both phases are of the order of 10^{-7}–10^{-8} $cm^2 \cdot s^{-1}$ (Fig. 2*D*), typical for lateral diffusion rates of lipids in the fluid phase (20). Based on the above analysis, it is concluded that the system shows the characteristic L_o/L_d phase coexistence. The difference in lipid mobility between the L_o and L_d phase is approximately a factor of 5 (averaged over the PC lipids), in agreement with experimental findings (5, 15, 21), which report factors of 2 to 10 depending on system details. In our simulations, the individual components can be easily traced. Whereas both PC lipids show very similar diffusion rates across the entire system, cholesterol appears to have a high relative diffusion rate in the disordered phase, which we attribute to its ability to readily flip-flop between the 2 leaflets. In the L_d phase, cholesterol flip-flop takes place on a submicrosecond time scale at a rate of $k = 5\ \mu s^{-1}$ (Fig. 2*D*). As a consequence, there is a non-negligible density of cholesterol residing in the membrane interior. This finding is in line with recent combined data (22) from simulation and neutron scattering experiments in which the cholesterol head group was found to be embedded in between the 2 leaflets for lipids containing 2 polyunsaturated tails. The apparent fast diffusion of cholesterol in the disordered domain arises from this membrane embedded population, which experiences the relative lower friction of the membrane interior (see Fig. S1). Diffusion of lipids and cholesterol is therefore partly decoupled in the L_d phase. In the raft-like L_o phase, on the other hand, cholesterol flip-flops do not occur on the time scale of the simulations, implying a strong coupling of the lateral mobility between the constituents. Flip-flop of lipids is not observed in either phase on the microsecond time scale. Exchange of lipids between the L_o and L_d phases, however, is observed frequently. The normalized per-unit length of the interface between the 2 phases, the exchange flux J is on the order of 10^{12} $cm^{-1} \cdot s^{-1}$, corresponding to 10–50 actual exchanges observed per lipid species (over the last 4 μs of the simulation across the total length of the interface, ≈40 nm). Rates for the saturated lipid ($J_{diC16\text{-}PC} = 1.4 \times 10^{12}$ $cm^{-1} \cdot s^{-1}$) are ≈3 times as high as for the unsaturated lipid ($J_{diC18:2\text{-}PC} = 0.4 \times 10^{12}$ $cm^{-1} \cdot s^{-1}$), mainly as a result of their relative concentration difference. Cholesterol exchanges significantly faster ($J_{CHOL} = 3.3 \times 10^{12}$ $cm^{-1} \cdot s^{-1}$), which we attribute to its enhanced diffusion rate.

Cholesterol's Preference for Saturated Tails Drives Phase Separation. Cholesterol is a key molecule in the formation of rafts, both in vivo and in vitro. Below ≈10 mol% cholesterol fluid–fluid phase separation is not observed in model ternary systems. Simulations of binary lipid mixtures without cholesterol indeed do not result in macroscopic fluid–fluid phase separation at the same state conditions, although the mixing of the 2 components is nonideal (Fig. S2*A*). Simulations of mixtures of diC_{16}-PC/$diC_{18:2}$-PC/cholesterol 0.28:0.42:0.3, on the other hand, show similar behavior as the 0.42:0.28:0.3 mixture described above (Fig. S2*B*). These results strongly suggest that the presence of cholesterol in this system is a prerequisite for coalescence of the nanodomains, resulting in macroscopic phase segregation. In connection to the special role of cholesterol, it is interesting to look in more detail at the lateral organization of cholesterol in the L_o phase. In Fig. 3*A*, a close-up of the system is shown revealing a typical cholesterol pattern, characterized by maximization of the contacts between cholesterol and the (saturated) lipid tails. The radial distribution function, shown in Fig. 3*B*, quantifies this behavior. A strong second peak is seen at a cholesterol–cholesterol distance of 1 nm, corresponding to a solvent-separated cholesterol pair. A smaller peak at 0.5 nm represents cholesterols in direct contact with each other. The occurrence of such cholesterol pairs, or higher-order aggregates, is suppressed compared with what is expected for a random distribution (Fig. 3*B*, *Inset*). The ratio of the first and second peak of the radial distribution function, 1:1.6, closely corresponds to that observed

in atomistic simulations of preassembled, raft-like mixtures (13). Because of the fluid nature of the L_o phase, at distances exceeding a few nanometers, any correlation is lost, as illustrated by the absence of long-range order in the radial distribution function.

Domain Boundary Between L_o and L_d Phases Is Diffuse at the Molecular Level. Although our simulations do not answer the question of why cholesterol and saturated lipids are attracted to each other, their co-condensation leads to domains differing strongly in both structural and dynamic properties. Apparently sharp on a macroscopic level, at the molecular level the domain boundary interface is rather diffuse. Restricting ourselves to the compositional measurement (Fig. 2*B*), this interfacial region is ≈5 nm wide, characterized by a composition in between that of the L_d and L_o phase. The broadness of the interface is largely a result of thermally induced capillary waves along the domain boundary. Based on fluctuation analysis (23), we estimate the associated line tension as 3.5 ± 0.5 pN, which is within the range of experimental values reported for ternary $diC_{18:1}$-PC/sphingomyelin/cholesterol mixtures at room temperature (4). Note that our estimate of the line tension is based on microscopic fluctuations that may also include contributions from the natural mixing gradient that exists between phase-separated domains. Especially close to the miscibility critical point, the line tension vanishes and the compositional mixing correlation length diverges. The large value of the line tension in our system implies that we are far from the critical point. An independent estimate of the line tension based on the pressure anisotropy in the system indeed gives a similar value compared to the fluctuation-based value, indicating that the dominant contribution arises from the capillary broadening. Details of these calculations are given in *SI Methods*.

Our simulations further reveal that the domain boundary interfaces opposing the raft-like domain exhibit larger fluctuations (Fig. 4 *A* and *B*) and therefore are energetically less costly. In terms of a line tension, the difference between the 2 types of interfaces is significant, 2.5 ± 0.3 pN vs. 4.5 ± 0.6 pN for the domain boundaries opposing the L_o and L_d phases, respectively. The existence of 2 types of interfaces is unanticipated and arises from the slight asymmetric registration of the domains (Fig. 4 *A* and *B*). Based on the compositional profiles for the individual monolayers (Fig. 2*B*), the difference in the average position of the boundaries is found to be ≈2 nm. These results predict the existence of a small, repulsive, effective interaction, possibly of entropic origin, between the domain boundary interfaces.

Domain Registration Is Caused by the Existence of a Small Domain Surface Tension. In addition to this domain interface repulsion, there must exist a counteracting driving force leading to the interleaflet colocalization (i.e., registration) of the domains, as seen in Figs. 1*C* and 2*A* and further quantified in Fig. 4*C*. Experiments on fluid–fluid phase-separated bilayers also show this domain registration (24). A plausible mechanism for monolayer coupling is the presence of a small surface tension between the 2 leaflets when the 2 different phases are in contact (25). Assuming that, for large mismatch areas, the dominant contribution to the free energy of the system arises from the surface tension of γ between the L_o and L_d phases, we can write $P(\Delta A) \approx e^{-\gamma \Delta A}$, with probability distribution $P(\Delta A)$ of the mismatch area ΔA. Fitting ln P in the regime of a large mismatch area (Fig. 4*D*) gives a surface tension of $\gamma = 0.15 \pm 0.05$ kT·nm^{-2}. Even such a small tension effectively suppresses overhang fluctuations larger than ≈20 nm^2 and therefore explains the registration of the domains on the macroscopic level probed experimentally. On the other hand, in real biological membranes the coupling is necessarily weaker because of the asymmetric lipid distribution, offering a possible explanation for the limited domain sizes seen in vivo.

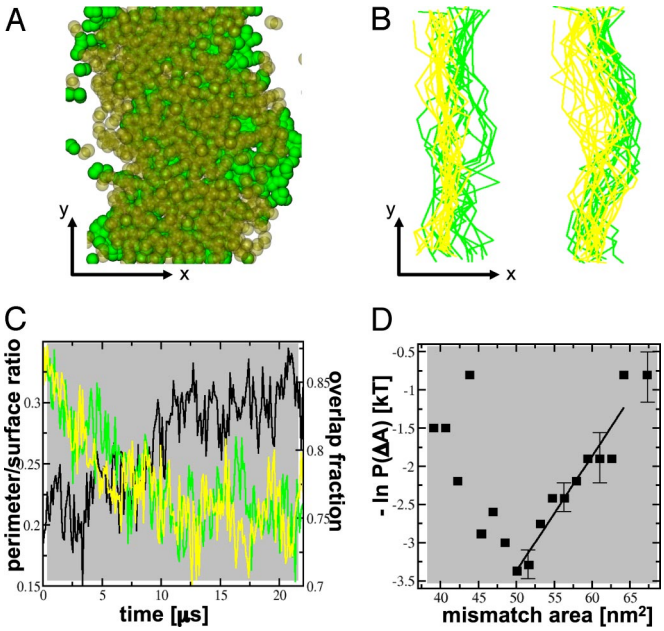

Fig. 4. Driving forces for domain formation. (*A*) Image showing the overlap of the 2 raft domains at the end of the simulation ($t = 20$ μs). Only the CG beads corresponding to the phosphate group (PCs) or hydroxyl group (cholesterol) are shown as green solid spheres for the lower monolayer and transparent yellow spheres for the upper monolayer. The direction across the domains is indicated by *x*, and the direction along the domains is indicated by *y*. (*B*) Overlaying instantaneous configurations of the domain interfaces in the upper (yellow) and lower (green) monolayer leaflets during the last 4 μs of the simulation. Note the difference in fluctuations for the 2 innermost interfaces, which oppose the L_o phase, vs. the outermost interfaces opposing the L_d domain. (*C*) Minimization of the perimeter of the domain interface for each of the 2 monolayers (yellow and green curves, left axis) and the increase in registration between the domains formed in both monolayer leaflets, expressed as the surface overlap fraction (black curve, right axis). (*D*) Logarithmic probability of the area mismatch vs. area mismatch. The solid line denotes a linear fit of the data in the high mismatch regime, from which the effective surface tension between the monolayer leaflets is estimated.

In summary, we showed that the phase coexistence of a L_o, raft-like domain, and a L_d, non-raft domain can be realistically simulated with a recently parameterized coarse-grained model. We should keep in mind, however, that the simulation model used here is a simplified one, lacking atomistic detail. It would be interesting to back-transform our equilibrated system to a fine-grained representation to verify our predictions. Our predictions include the existence of a small surface tension between the domains, driving their registration, and a short-ranged line repulsion between the domain boundaries. Although many questions remain, simulations such as presented in the current work will hopefully aid in our understanding of the nature of lipid rafts, and to many related cell membrane processes such as the self-assembly of functional protein complexes.

Methods

The MARTINI Model. All systems were simulated with the MARTINI CG force field (11), version 2.0. The MARTINI model has been parameterized extensively over the past 5 years by using a chemical building block principle. The key feature is the reproduction of thermodynamic data, especially the partitioning of the building blocks between aqueous and oil phases. In a series of applications (26–29) the model has been shown to reproduce many properties of lipid membranes. The MARTINI model uses a 4-to-1 mapping; i.e., on average, 4 heavy atoms are represented by a single interaction center, with an exception for ring-like molecules such as cholesterol that are mapped with

somewhat higher resolution (≈3-to-1). Solvent is explicitly included. The interactions between the CG sites are modeled by a set of short-ranged Lennard–Jones potentials. Charged groups such as the zwitterionic lipid head groups also interact via a Coulombic energy function. In addition, a set of bonded potentials is used to describe the chemical connectivity of the molecules. Parameters for polyunsaturated chains were not available and have been optimized by using the all-atom simulations of Feller *et al.* (30). More details about the MARTINI force field, including some specific parameterization required for the current study, are given in *SI Methods*. The parameters and example input files of the simulations described in this paper are available at http://md.chem.rug.nl/~marrink/coarsegrain.html.

Simulation Details. The simulations described in this paper were performed with the GROMACS simulation package (31), version 3.3. In all simulations the solvent molecules, lipids, and cholesterol were independently coupled to a constant temperature bath (32) with a relaxation time of $\tau_T = 0.1$ ps. Based on exploratory simulations, a target temperature of 295 K was chosen as an optimal value to observe clear phase separation on an accessible time scale. A higher temperature brings the system closer to the critical point, which might be more realistic for the state of membranes in vivo, but prevents the clear analysis of domain properties as presented here. Lower temperatures, on the other hand, slow down the equilibration of the 2 phases. The pressure was weakly coupled (32) to 1 bar with a relaxation time of $\tau_P = 0.5$ ps. For the planar membranes the pressure coupling used a semiisotropic scheme in which the (*x*, *y*) plane and the *z* direction were coupled separately. This approach resulted in a tensionless bilayer. For the vesicular system we used the Mean Field Force Approximation boundary (MFFA) approach (33), which reduces the number of degrees of freedom in the system by removing the bulk water surrounding the vesicle. More details of the MFFA approach in applications involving vesicular systems can be found in the original publication (33).

All planar systems were simulated for 18×10^7 steps, and the vesicular system was simulated for 3.5×10^7 steps, by using an integration time step of 30 fs and an update of the neighbor list every 10 steps. Because of the smoothness of the CG potentials, the effective time scale sampled is larger than the actual simulation time. Based on a comparison of diffusion constants in CG systems and systems modeled at atomic detail, the effective time sampled by the CG model was found to be 2- to 10-fold larger (11). When interpreting the simulation results with the CG model, one can find a first approximation simply by scaling the time axis. The standard conversion factor we used is a factor of 4, which is the speed-up factor in the diffusional dynamics of CG water compared with real water. A similar scaling factor appears to describe the general dynamics present in a variety of systems quite well. The time scale quoted here is therefore an effective time scale, which should be interpreted with care. The total effective time sampled was slightly >20 μs for each of the planar membrane systems and 4 μs for the vesicular system. Equilibration of the systems was monitored by looking at the system energy and various structural properties, including the domain perimeter and domain coupling. The vesicular system did not reach a fully equilibrated state, and therefore no attempts were made to analyze this system in more detail. For the lamellar systems, during the last 4 μs of simulation no significant changes in system properties occurred, and therefore the system was considered to be equilibrated (see Fig. 4*C*, showing the temporal evolution of the domain perimeter and coupling).

System Set-Up. Initially, a small, equilibrated patch of a binary diC_{16}-PC/cholesterol mixture was obtained from previous studies (11). This patch contained 38 diC_{16}-PC and 16 cholesterol molecules (0.3 mol fraction of cholesterol). The hydration level was 350 CG water beads, corresponding to 26 real waters per lipid. To construct the ternary mixture, 15 of the diC_{16}-PC molecules were transformed into $diC_{18:2}$-PC molecules. After short energy minimization to release the stress caused by the different topology of some of the tails, the small membrane patches were equilibrated for 100 ns at an elevated temperature of 400 K to randomize the lateral organization. Subsequently, the system was copied 6 times in both lateral directions to obtain the final systems, containing 828 diC_{16}-PC, 540 $diC_{18:2}$-PC, 576 cholesterols, and 12,600 water beads. The molar composition of this mixture was diC_{16}-PC/$diC_{18:2}$-PC/cholesterol 0.42:0.28:0.3. This step was followed by a short, 10-ns simulation at the target temperature of 295 K with increased coupling to the temperature and pressure baths to relax the overall system size close to its equilibrium value. This is considered the starting point (*t = 0*) of the simulations presented in this article. The diC_{16}-PC/$diC_{18:2}$-PC/cholesterol 0.28:0.42:0.3 ternary mixture was obtained by using the same procedure, replacing 23 of the diC_{16}-PC by $diC_{18:2}$-PC lipids initially.

Simulations of binary diC_{16}-PC/$diC_{18:2}$-PC systems in the range 6:1 to 1:3 were prepared starting from pure diC_{16}-PC bilayer patches. To verify the reproducibility of our results, control simulations were performed for each of these systems, by using 4× smaller system sizes and different starting conditions. In each case, the ternary mixtures completely phase-separated, whereas the binary systems did not, at least at the temperature of study (295 K). Cooled further, binary mixtures showed gel/fluid coexistence (H.J.R. and S.J.M., unpublished data). To quantify the lateral mobilites of the 2 populations for cholesterol in the L_d phase, a separate simulation of a small bilayer patch approximately matching the composition of the L_d phase was performed. This system, composed of 128 $diC_{18:2}$-PC lipids and 35 cholesterols, was simulated for 1 μs at $T = 295$ K.

The vesicle used in this study was formed by spontaneous aggregation of the lipid components within the MFFA boundary set-up, as follows. We randomly inserted 1,250 diC_{16}-PC, 730 $diC_{18:2}$-PC, and 834 cholesterol molecules in a sphere with a 12.5 nm radius, respecting the excluded volume of each bead. The remaining volume of the shell was subsequently filled with CG water beads. In total, 49,003 CG water beads were added. The system was initially run at a temperature of 323 K. Aided by the molding effect of the spherical boundary, rapid formation of a vesicle was observed. After 30 ns, when the overall shape of the vesicle had appeared but several pores still remained in the vesicle, the temperature was quenched to the target temperature of 295 K allowing the vesicle to equilibrate at the desired conditions. After ≈100 ns the vesicle had completely sealed. This state corresponds to $t = 0$ μs in Fig. 1*C*.

Method of Analysis. Details of the methods of analysis and error estimation can be found in *SI Methods*.

ACKNOWLEDGMENTS. We thank H. J. C. Berendsen, A. H. de Vries, B. Poolman, T. Baumgart, and S. R. Wassall for helpful discussions. This work was supported by the Molecule-to-Cell program of the Netherlands Organization for Scientific Research.

1. Jacobson K, Mouritsen OG, Anderson RGW (2007) Lipid rafts: At a crossroad between cell biology and physics. *Nat Cell Biol* 9:7–14.
2. Simons K, Ikonen E (1997) Functional rafts in cell membranes. *Nature* 387:569–572.
3. Dietrich C, Volovyk ZN, Levi M, Thompson NL, Jacobson K (2001) Partitioning of Thy-1, GM1, and cross-linked phospholipid analogs into lipid rafts reconstituted in supported model membrane monolayers. *Proc Natl Acad Sci USA* 98:10642–10647.
4. Baumgart T, Hess ST, Webb WW (2003) Imaging coexisting fluid domains in biomembrane models coupling curvature and line tension. *Nature* 425:821–824.
5. Kahya N, Scherfeld D, Bacia K, Poolman B, Schwille P (2003) Probing lipid mobility of raft-exhibiting model membranes by fluorescence correlation spectroscopy. *J Biol Chem* 278:28109–28115.
6. Samsonov AV, Mihalyov I, Cohen FS (2001) Characterization of cholesterol-sphingomyelin domains and their dynamics in bilayer membranes *Biophys J* 81:1486–1500.
7. Zhao J, *et al.* (2007) Phase studies of model biomembranes: Complex behavior of DSPC/DOPC/cholesterol. *Biochim Biophys Acta Biomembr* 1768:2764–2776.
8. Baumgart T, *et al.* (2007) Large-scale fluid/fluid phase separation of proteins and lipids in giant plasma membrane vesicles. *Proc Natl Acad Sci USA* 104:3165–3170.
9. Lingwood D, Ries J, Schwille P, Simons K (2008) Plasma membranes are poised for activation of raft phase coalescence at physiological temperature. *Proc Natl Acad Sci USA* 105:10005–10010.
10. Veatch SL, *et al.* (2008) Critical fluctuations in plasma membrane vesicles. *ACS Chem Biol* 3:287–293.
11. Marrink SJ, Risselada HJ, Yefimov S, Tieleman DP, de Vries AH (2007) The MARTINI force field: Coarse grained model for biomolecular simulations *J Phys Chem B* 111:7812–7824.
12. Ayton GS, McWhirter JL, McMurtry P, Voth GA (2005) Coupling field theory with continuum mechanics: A simulation of domain formation in giant unilamellar vesicles. *Biophys J* 88:3855–3869.
13. Niemela PS, Ollila S, Hyvonen MT, Karttunen M, Vattulainen I (2007) Assessing the nature of lipid raft membranes *PLoS Comp Biol* 3:304–312.
14. Pandit S, Jakobsson E, Scott HL (2004) Simulation of the early stages of nano-domain formation in mixed bilayers of sphingomyelin, cholesterol, and dioleylphosphatidylcholine. *Biophys J* 87:3312–3322.
15. Filippov A, Orädd G, Lindblom G (2007) Domain formation in model membranes studied by pulsed-field gradient-NMR: The role of lipid polyunsaturation. *Biophys J* 93:3182–3190.
16. Soni SP, *et al.* (2008) Docosahexaenoic acid enhances segregation of lipids between raft and non-raft domains: ^{2}H NMR study. *Biophys J* 95:203–214.
17. Huang J, Buboltz JT, Feigenson GW (1999) Maximum solubility of cholesterol in phosphatidylcholine and phosphatidylethanolamine bilayers. *Biochim Biophys Acta Biomembr* 1417:89–100.
18. Veatch SL, Polozov IV, Gawrisch K, Keller SL (2004) Liquid domains in vesicles investigated by NMR and fluorescence microscopy. *Biophys J* 86:2910–2922.
19. Rinia HA, Snel MME, van der Eerden JPJM, de Kruijff B (2001) Visualizing detergent resistant domains in model membranes with atomic force microscopy. *FEBS Lett* 501:92–96.

20. Lindblom G, Orädd G (1994) NMR Studies of translational diffusion in lyotropic liquid crystals and lipid membranes. *Progr Nucl Magn Res Spectr* 26:483–515.
21. Almeida PF, Vaz WL, Thompson TE (1993) Percolation and diffusion in 3-component lipid bilayers - Effect of cholesterol on an equimolar mixture of 2 phosphatidylcholines. *Biophys J* 399:399–412.
22. Marrink SJ, de Vries AH, Harroun TA, Katsaras J, Wassall SR (2008) Cholesterol shows preference for the interior of polyunsaturated lipid. *J Am Chem Soc* 130:10–11.
23. Esposito C, *et al*. (2007) Flicker spectroscopy of thermal lipid bilayer domain boundary fluctuations. *Biophys J* 93:3169–3181.
24. Bagatolli LA, Gratton E (2001) Direct observation of lipid domains in free-standing bilayers using two-photon excitation fluorescence microscopy. *J Fluoresc* 11:141–160.
25. Collins MD (2008) Interleaflet coupling mechanisms in bilayers of lipids and cholesterol *Biophys J* 94:L32–L34.
26. Marrink SJ, de Vries AH, Mark AE (2004) Coarse grained model for semiquantitative lipid simulations. *J Phys Chem B* 108:750–760.
27. Marrink SJ, Mark AE (2004) Molecular view of hexagonal phase formation in phospholipid membranes. *Biophys J* 87:3894–3900.
28. Marrink SJ, Risselada J, Mark AE (2005) Simulation of gel phase formation and melting in lipid bilayers using a coarse grained model. *Chem Phys Lip* 135:223–244.
29. Faller R, Marrink SJ (2004) Simulation of domain formation in DLPC-DSPC mixed bilayers. *Langmuir* 20:7686–7693.
30. Feller SE, Gawrisch K, MacKerell AD, Jr (2002) Polyunsaturated fatty acids in lipid bilayers: Intrinsic and environmental contributions to their unique physical properties *J Am Chem Soc* 124:318–326.
31. van der Spoel D, *et al*. (2005) GROMACS: Fast, flexible and free. *J Comput Chem* 26:1701–1718.
32. Berendsen HJC, Postma JPM, van Gunsteren WF, DiNola A, Haak JR (1984) Molecular-dynamics with coupling to an external bath. *J Chem Phys* 81:3684–3690.
33. Risselada HJ, Mark AE, Marrink SJ (2008) The application of mean field boundary potentials in simulations of lipid vesicles. *J Phys Chem B* 112:7438–7447.